Nickel Catalysts Supported on SiO_2-CeO_2 Mixed Oxides for Methane Dry Reforming

Carla Calabrese , Valeria La Parola * , Giuseppe Pantaleo , Leonarda Francesca Liotta *

Posted Date: 14 January 2026

doi: 10.20944/preprints202601.0953.v1

Keywords:

Ni over SiO_2-CeO_2 mixed oxides; CeO2 loading; preparation method; methane dry reforming; coke resistance

 doi:10.20944/preprints202601.0953.v1

Article

Nickel Catalysts Supported on SiO_2-CeO_2 Mixed Oxides for Methane Dry Reforming

Carla Calabrese, Valeria La Parola *, Giuseppe Pantaleo and Leonarda Francesca Liotta *

Institute for the Study of Nanostructured Materials (ISMN)-CNR, Via Ugo La Malfa 153, 90146 Palermo, Italy

* Correspondence: valeria.laparola@cnr.it (V.L.P.); leonardafrancesca.liotta@cnr.it (L.F.L.)

Abstract

Nickel-supported over SiO_2-CeO_2 mixed oxides were investigated as catalysts for syngas production via the dry reforming of methane. The SiO_2-CeO_2 supports were optimized, playing on the preparation method and ceria loading with the aim of stabilizing nickel nanoparticles, enhancing the catalytic performance, and improving the resistance to coke formation under high-temperature reforming conditions. To investigate the effect of support composition, SiO_2-CeO_2 mixed oxides with ceria contents ranging from 5 to 30 wt% were prepared using two synthesis routes: sol-gel and wetness impregnation methods. A nickel loading of 5 wt% was deposited on the resulting supports. The catalysts were characterized by XRD, N_2 physisorption, temperature-programmed reduction, and Raman spectroscopy. Catalytic activity tests were conducted over reduced catalysts in an H_2-He stream at 750 °C, using a feed mixture containing 15 vol% CH_4 and 15 vol% CO_2 in He. The effect of temperature on catalytic performance was evaluated in the range of 450–800 °C. Thermogravimetric, XRD and Raman analyses of spent catalysts were used to assess carbon deposition and the nature of crystalline phases. The results highlight the role of CeO_2 content and preparation method in determining nickel dispersion, reducibility, catalytic performance in DRM, and coke resistance.

Keywords: Ni over SiO_2-CeO_2 mixed oxides; CeO_2 loading; preparation method; methane dry reforming; coke resistance

1. Introduction

Greenhouse gas emissions from fossil fuel combustion and industrial processes have emerged as a primary driver of the current environmental crisis. The increasing atmospheric concentration of pollutants such as carbon dioxide and methane results in a pronounced climate change. Addressing this crisis requires a transition to low-carbon energy systems combined with coordinated international policy efforts to ensure long-term environmental sustainability[1]. This challenge has motivated the development of catalytic technologies designed to convert greenhouse gases into valuable chemical feedstocks. In this scenario, the dry reforming of methane (DRM: $CH_4 + CO_2 \rightarrow 2H_2 + 2CO$) has attracted growing attention because it simultaneously consumes CH_4 and CO_2 to produce synthesis gas ($CO + H_2$), a key intermediate for downstream processes such as Fischer-Tropsch synthesis, methanol synthesis, and hydrocarbon upgrading[2,3]. However, the practical implementation of DRM faces significant challenges, including the high temperatures required to activate stable reactants and the catalysts deactivation through carbon deposition and metal sintering[4,5].

Nickel-based catalysts are widely regarded as the most economical and industrially viable materials for DRM, offering high intrinsic activity for C–H bond activation at a significantly lower cost than noble metals such as Ru, Rh, or Pt[6]. Nevertheless, their application remains limited by rapid deactivation caused by carbon formation[7], the growth and agglomeration of Ni nanoparticles, and interactions leading to inactive phases. To mitigate these issues, the development of advanced materials that can stabilize Ni particles, improve reducibility, and enhance coke resistance has become a key research focus[8–10]. Among the reported catalytic systems for methane dry reforming,

 doi:10.20944/preprints202601.0953.v1

CeO_2 has emerged as a promising support for Ni active sites owing to its excellent redox properties and oxygen storage capacity, which promote the removal of carbon deposits, enhance catalyst stability, and mitigate coke formation[11–13]. The Ce^{3+}/Ce^{4+} redox cycle enables lattice oxygen to participate in the oxidation of CH_4, generating oxygen-deficient CeO_{2-x} species that can be reoxidized by CO_2, thus preserving the catalytic performance and extending the lifetime of the Ni/CeO_2 catalytic system.

Hybrid SiO_2-CeO_2 mixed oxides represent a particularly attractive support for Ni-based catalysts[14–16]. Silica provides high surface area, thermal stability, and well-controlled porosity[17,18], while ceria contributes oxygen mobility and redox activity that facilitate carbon oxidation and CO_2 activation[19]. The combination of these two oxides can therefore enhance nickel dispersion, strengthen metal-support interactions, and improve resistance to carbon deposition during DRM[20,21]. Importantly, both the ceria content and the support synthesis method significantly influence the physicochemical properties of SiO_2-CeO_2 systems, affecting parameters such as surface area, degree of Ni-support interaction, oxygen vacancy concentration, and reducibility[22–24].

In this study, we systematically investigate the influence of CeO_2 content (5-30 wt%) and the support synthesis method (sol-gel *vs.* wetness impregnation) on the structural, textural, and catalytic properties of Ni/SiO_2-CeO_2 catalysts for methane dry reforming. SiO_2-CeO_2 composites were prepared using either sol-gel route or wetness impregnation, followed by the incorporation of nickel *via* wetness impregnation. Comprehensive physicochemical characterization, including X-ray diffraction (XRD), N_2 physisorption, and H_2 temperature-programmed reduction (H_2-TPR), was performed to elucidate structural evolution, porosity, and reducibility. Catalytic performance was evaluated between 450 and 800 °C using a CH_4/CO_2 mixture, and spent catalysts were examined by thermogravimetric analysis (TG) and XRD to evaluate carbon deposition and phase stability. By correlating preparation methods, ceria content, and reaction performance, this work provides new insight into the design of Ni-based catalysts with enhanced coke resistance and improved stability for DRM.

2. Results and Discussion

SiO_2-CeO_2 mixed oxides (SiCe) were developed as supports for Ni-based catalysts to be used in syngas production via methane reforming with carbon dioxide. These SiCe supports were designed to stabilize Ni dispersed nanoparticles, with enhanced catalytic activity and improved resistance to coke formation during high-temperature reforming process.

SiCe powders were synthesized using two distinct strategies: the sol-gel route (SiCe5-30-SG) and the wetness impregnation method (SiCe5,30-WI).

To investigate the influence of support composition, four SiCe materials with ceria contents of 5, 10, 20, and 30 wt% were synthesized using the sol-gel method. A pure SiO_2 support was also prepared both as a reference material and as the bare support for the synthesis of two additional SiCe supports with CeO_2 contents of 5 and 30% by the wetness impregnation method (SiCe5-WI, SiCe30-WI).

The supported Ni catalysts (5 wt%), prepared by wetness impregnation of SiCe powders, were labeled as NiSi, NiSiCe5-SG, NiSiCe10-SG, NiSiCe20-SG, NiSiCe30-SG, NiSiCe5-WI, and NiSiCe30-WI.

Ni catalysts were analyzed by X-ray powder diffraction (Figure 1) to investigate the structural properties. The recorded patterns of most samples display the characteristic reflections of CeO_2 at 28.5°, 33.0°, 47.5°, and 56.3° 2θ, assigned to the (111), (200), (220), and (311) planes of its fluorite-type cubic structure (ICSD No. 28753, space group *Fm–3m*).

In contrast, when the sol-gel method was applied to prepare the material with the lowest CeO_2 content, NiSiCe5-SG, the corresponding XRD pattern shows barely visible CeO_2 diffractions, suggesting the presence of ceria as highly dispersed phase as well as fine nanometric domains embedded within the amorphous silica network. The XRD patterns of the calcined catalysts clearly

 doi:10.20944/preprints202601.0953.v1

display NiO reflections consistent with ICSD reference No. 24018. The primary NiO peaks are detected at 37.2°, 43.3°, and 62.9° 2θ, corresponding to the (111), (200), and (220) planes, respectively. Interestingly, as the ceria content increases, these peaks become less intense and broader, indicating that NiO particles are more finely dispersed on the supports with higher CeO_2 loadings.

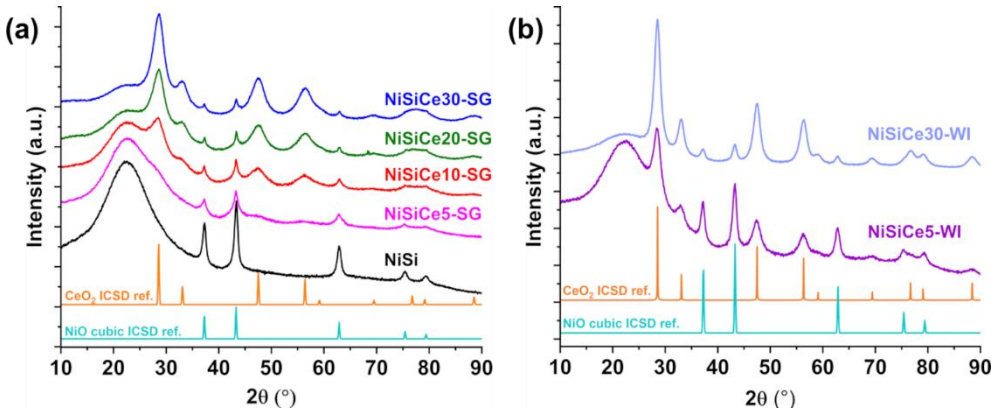

Figure 1. XRD patterns of as prepared catalysts: (a) NiSi and NiSiCe(5-30)-SG, (b) NiSiCe(5,30)-WI along with CeO_2 ICSD reference (No. 28753) and NiO ICSD reference (No. 24018).

NiO mean crystal sizes were calculated by Scherrer equation, and the values are listed in Table 1. An effect of the catalyst composition on the structural properties was observed. NiSi, without ceria, exhibits the largest NiO crystallite size (22.7 nm). With the incorporation of CeO_2 into the silica matrix a systematic reduction in NiO crystallite size was observed. At low ceria loadings (NiSiCe5-SG and NiSiCe10-SG), the NiO mean size decreases to approximately 17.0-16.6 nm, followed by a further reduction to 15.7 nm for NiSiCe20-SG. The smallest NiO crystallites (11.8 nm) were obtained for NiSiCe30-SG. This progressive decrease in NiO crystallite size suggests that the presence of ceria effectively inhibits NiO crystal growth, likely because of strengthened metal-support interactions and enhanced dispersion of Ni species promoted by CeO_2. A similar effect was registered also for the wet impregnated samples, NiSiCe5-WI, and NiSiCe30-WI, showing smaller and better dispersed NiO crystallites at higher CeO_2 loadings.

N_2 physisorption measurements were performed on the investigated catalysts to evaluate their textural properties, including specific surface area (SSA), pore volume and mean pore size (Table 1). The specific surface area (SSA) of the catalysts differs significantly based on the CeO_2 content and the preparation method. The bare silica-supported catalyst (NiSi) shows a high surface area of 242 m^2/g, a pore volume of 0.50 cm^3/g, and a mean pore diameter of 16.4 nm. When CeO_2 is incorporated using the sol-gel method, there is a notable impact on the textural properties. At a low CeO_2 content (NiSiCe5-SG), the SSA increases to 310 m^2/g; however, the pore volume decreases significantly to 0.16 cm^3/g, and the mean pore diameter drops to 2.73 nm. This suggests the formation of a finer pore structure, likely due to the well-dispersed ceria within the silica matrix. When the CeO_2 content is increased further (NiSiCe10-30-SG), there is a gradual reduction in surface area and pore volume, accompanied by a slight increase in pore diameter at higher loadings. This likely indicates a modification of the pore structure or aggregation of the CeO_2 particles. On the other hand, catalysts prepared by wetness impregnation (NiSiCe5-WI and NiSiCe30-WI) maintain higher pore volumes (0.48-0.52 cm^3/g) and larger pore sizes (14.9-17.7 nm), which reflects the preservation of the original silica pore structure. These findings suggest that the preparation method plays a significant role in the dispersion of CeO_2 and the resulting textural properties of the Ni/SiO_2-CeO_2 catalysts.

 doi:10.20944/preprints202601.0953.v1

Table 1. Specific surface area, pore volume, pore size, and crystal size of the investigated catalysts.

Sample	SSA (m^2/g)	Pore Volume (cm^3g^{-1})	BJH mean pore size (nm)	NiO crystal size [1] (nm)
NiSi	242	0.50	16.4	22.7
NiSiCe5-SG	310	0.16	2.73	17.0
NiSiCe10-SG	230	0.12	2.85	16.6
NiSiCe20-SG	149	0.10	3.12	15.7
NiSiCe30-SG	163	0.12	4.18	11.8
NiSiCe5-WI	275	0.48	17.7	19.0
NiSiCe30-WI	228	0.52	14.9	11.0

[1] Calculated by Scherrer equation.

Hydrogen temperature-programmed reduction (H_2-TPR) analysis was performed on Ni-supported catalysts to investigate the effect of ceria content on the reducibility and Ni-support interactions. The observed features reflect the reduction of Ni^{2+} to Ni^0 and Ce^{4+} to Ce^{3+} (Figure 2) as confirmed by the experimental H_2 consumption values that are in agreement with full reduction of Ni^{2+} to metallic Ni and reduction of Ce^{4+} to Ce^{3+}, that completely occurs at ceria loadings ≤ 10 wt%.

NiO particles with moderate interaction with the support are reduced in the range of 300-400 °C, whereas NiO strongly interacting with the support occurs at higher temperatures. The TPR profile of NiSi shows broad asymmetric peaks centred at ~350 °C and ~600°C, whereas the high-temperature peak can be ascribed to the reduction of small NiO particles strongly interacting with the silica surface, which are difficult to reduce, while the low-temperature peak corresponds to larger NiO crystallites with weaker interaction, more characteristic of bulk NiO[24,25].

CeO_2-containing catalysts display further reduction features between 400 and 700 °C, which can be assigned to the reduction of surface and bulk ceria ($Ce^{4+} \rightarrow Ce^{3+}$).

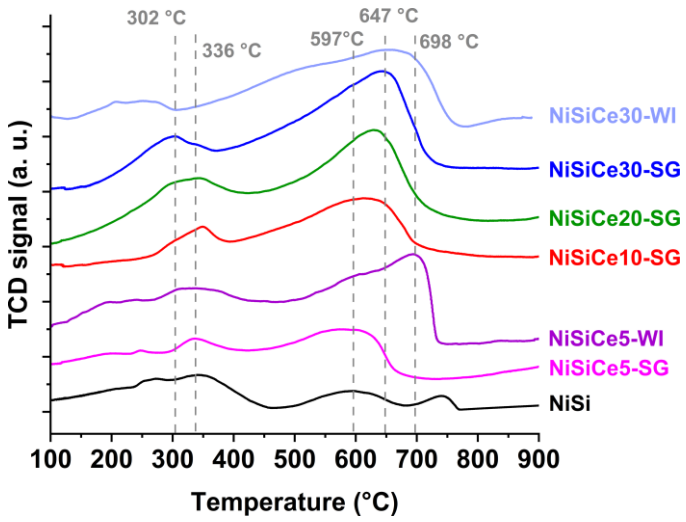

Figure 2. H_2-TPR profiles of Ni-based catalysts.

The catalytic activity of the NiSiCe(5-30)-SG catalysts was evaluated in the dry reforming of methane (DRM) reaction under temperature-gradient conditions ranging from 450 to 750 °C (Scheme 1, Figure 3). The results indicate an increase in CH_4 conversion in the following order: NiSi > NiSiCe5-SG > NiSiCe20-SG > NiSiCe30-SG > NiSiCe10-SG.

 doi:10.20944/preprints202601.0953.v1

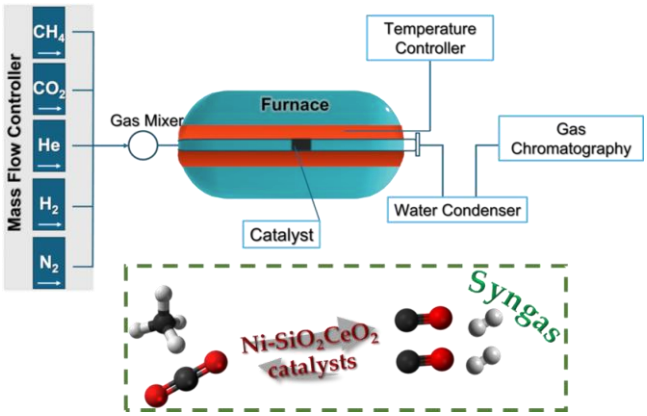

Scheme 1. Representation of DRM experimental set-up.

The highest activity of NiSi can be related to the presence of NiO particles resulting in weaker metal-support interactions. These features allow more reducible Ni species, which improve the overall catalytic activity. A high catalytic activity was noted for the material with the lowest CeO_2 content NiSiCe5-SG. This could likely be attributed to the combination of well-dispersed ceria domains and the presence of moderately interacting NiO species, as indicated by H_2-TPR analysis. Additionally, the improved oxygen mobility linked to finely dispersed ceria may also facilitate enhanced carbon removal (see TGA profile, Figure 4a), contributing to sustained catalytic activity.

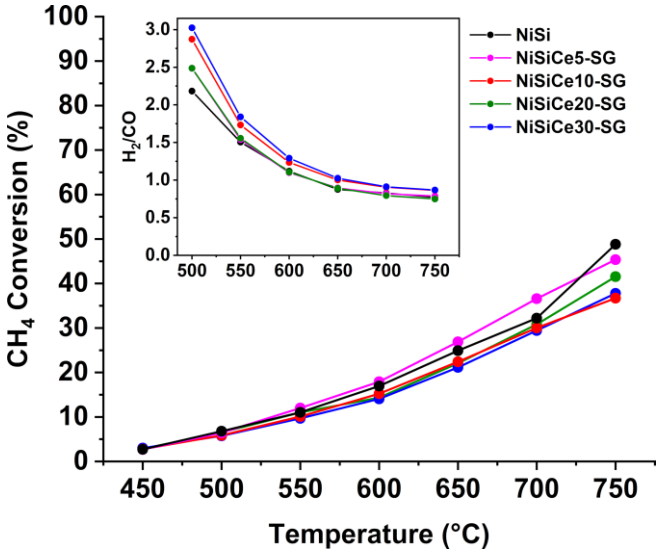

Figure 3. DRM results for NiSi and NiSiCe5-30-SG catalysts: CH_4 conversion and H_2/CO molecular ratio (inset) as a function of temperature between 450-750 °C.

As the CeO_2 content increases beyond 10 wt%, the catalytic activity decreases. This behaviour can be due to the stronger Ni-support interactions induced by ceria, which lead to the formation of highly stabilized and less reactive NiO species. These factors can limit the amount of active Ni^0 available on the surface of the catalyst under reaction conditions. Interestingly, the NiSiCe30-SG catalyst performs better than NiSiCe20-SG for CO_2 conversion but shows slightly reduced performance in methane conversion. This suggests that oxygen mobility and CO_2 activation, both promoted by higher ceria contents, compensate partially for the stronger metal-support interaction at elevated CeO_2 loading.

The results demonstrate that the catalytic performance of the NiSiCe(5-30)-SG series is strongly influenced by the ceria content, which affects Ni dispersion, reducibility, and the extent of Ni-support interactions. Lower ceria contents promote, upon reduction, the formation of active Ni^0 species while

 doi:10.20944/preprints202601.0953.v1

still providing enough redox functionality to assist in carbon removal. Higher ceria loadings likely promote strong interactions between oxidized NiO species and the ceria bulk, rendering the Ni active sites poorly accessible on the catalyst surface and consequently reducing catalytic activity. Figure 3 (inset) reports the H_2/CO molecular ratio values as a function of temperature in the range 500-750 °C.

The H_2/CO values decreased with increasing temperature, dropping from above 2 at 500 °C to approximately 1-0.8 in the 650-750 °C range. The temperature-dependent evolution of the H_2/CO ratio can be attributed to the occurrence of additional reactions during the DRM test[6]. Specifically, the exothermic Boudouard reaction ($2CO \leftrightarrow C + CO_2$), which is favored at lower temperatures, leads to CO consumption, and thus contributes to the higher H_2/CO ratio. In contrast, endothermic reactions such as the reverse Boudouard reaction and the reverse water-gas shift (RWGS) reaction ($CO_2 + H_2 \leftrightarrow CO + H_2O$) enhance CO formation at higher temperatures, thereby reducing the H_2/CO molar ratio[6,25,26].

After DRM reaction, the spent catalysts were characterized by TGA and XRD analyses. The extent of carbon deposition on the spent NiSi and NiSiCe (5-30)-SG catalysts was determined by thermogravimetric (TG) analysis, as shown in Figure 4a. The weight losses associated with carbon combustion ranged from approximately 18.5 wt% for NiSiCe5-SG to 2.8 wt% for the least active NiSiCe10-SG. Carbon oxidation occurred within the temperature range 586-703 °C, indicating, for NiSi, the coexistence of carbon species with different structural features (*e.g.*, amorphous carbon). These results highlight the correlation between catalytic performance and carbon formation.

According to the TG analysis, the XRD patterns of NiSiCe (5-30)-SG powders after DRM under a temperature gradient show a diffraction peak at 26.5° (2θ), corresponding to graphitic carbon (Figure 4b). In addition, metallic nickel was clearly detected in the spent catalysts, identified by the (111), (200), and (220) reflections at 2θ = 44.4°, 51.8°, and 76.3°, respectively. The absence of CeO_2 diffraction peaks after DRM was observed for all the samples and has also been reported in the literature for Ni/SiO_2–CeO_2 catalysts[27,28]. This result was ascribed to the catalyst reduction pre-treatment at 750 °C under 5% H_2/He carried out before DRM test. The reducing atmosphere induced $Ce^{4+} \rightarrow Ce^{3+}$ reduction and the formation of oxygen vacancies, disrupting the long-range crystallinity of the fluorite structure.

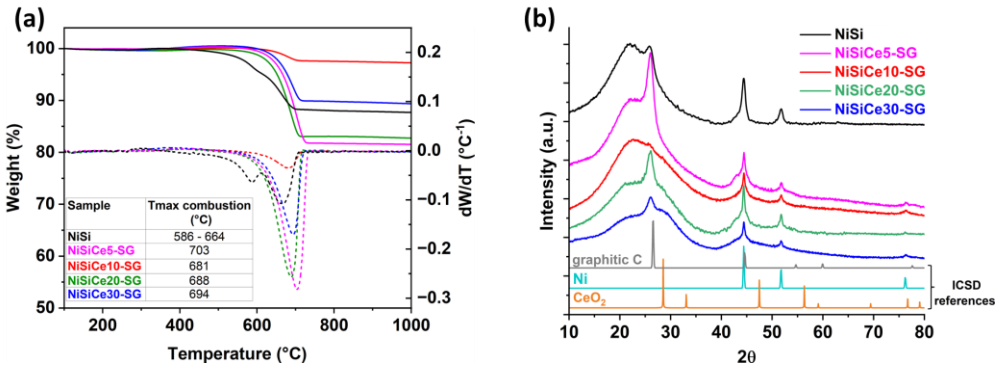

Figure 4. Characterization of the NiSi and NiSiCe(5-30)-SG spent catalysts: (a) TG (solid line) and DTG (dashed line) profiles; (b) XRD patterns of the spent NiSi and NiSiCe(5-30)-SG, ICSD references (metallic Ni No. 125689, CeO_2 No. 28753, graphitic C No. 145395).

Given the high catalytic activity of NiSi observed during the DRM carried out at gradient temperature, together with the limited extent of carbon deposition, a long-term stability test was conducted at 700 °C for 24 h after prior reduction at 750 °C for 1 h under a flow of 5% H_2/He. As shown in Figure 5, both CH_4 and CO_2 conversions exhibit a slight increase during the initial hours on stream, followed by stable values over the entire 24 h time-on-stream test. CO_2 conversion values were higher than those recorded for CH_4. This behaviour is consistent with the literature and can be explained by the occurrence of the reverse water gas shift reaction (RWGS: $CO_2 + H_2 \leftrightarrow CO + H_2O$)[25].

 doi:10.20944/preprints202601.0953.v1

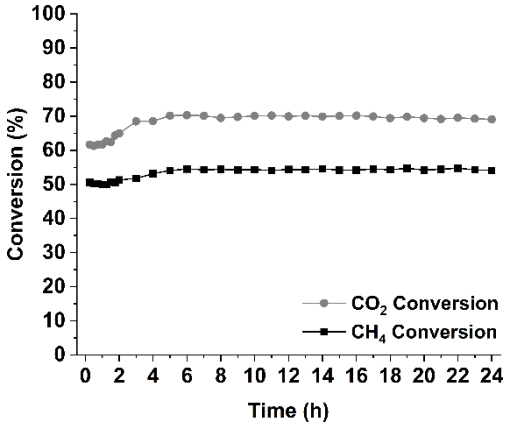

Figure 5. DRM long run test at 700 °C for NiSi catalyst.

CO_2 conversion rapidly reaches approximately 70% and remains essentially constant thereafter, indicating steady catalytic performance. Likewise, CH_4 conversion increases to about 55% in the early stage of the reaction and subsequently stabilizes, with no evidence of deactivation. The absence of any progressive decline in conversion for either reactant points to good catalyst stability under the investigated conditions and is consistent with the limited carbon deposition observed during the test at gradient temperature.

In order to verify the hypothesis that NiSiCe-SG catalysts exhibit lower activity than the corresponding NiSi sample due to the strong Ni-CeO_2 interaction, the catalyst with the highest ceria content, NiSiCe30-SG, was subjected to a redox treatment (TPR-TPO-TPR). In details, after a first TPR, the sample was oxidized from room temperature up to 600 °C (hold time 1h) using a 5% O_2/He mixture (v/v, 30 mL/min), then cooled to room temperature under helium and, finally, a second TPR was registered. This procedure was carried out to investigate changes in the reducibility of oxidized Ni species. In Figure 6a, the second reduction profile was compared with the first one, already shown in Figure 2. An evident change of the second reduction profile of NiSiCe30-SG was registered in comparison with the first TPR. After the redox treatment (TPR-TPO-TPR), the second H_2-TPR profile shows a marked shift of the main reduction feature toward lower temperatures, with the maximum now centered around 450-500 °C and a narrower distribution of reduction peaks. This behavior suggests a partial weakening of the metal-support interaction and an increased fraction of more easily reducible Ni^{2+} and Ce^{4+} species formed upon reoxidation. The enhanced reducibility, observed in the second TPR, indicates that the redox cycling modifies the nature of the Ni species, likely promoting changes at the Ni-CeO_2 interface, which may have implications for the catalytic performance of the NiSiCe30-SG system. Based on the so far reported results, a fresh portion of the NiSiCe30-SG catalyst was subjected to a first reduction at 750 °C for 1 h under 5% H_2/He, then after cooling to room temperature under inert gas, the sample was oxidized at 600 °C 1h, therefore, again reduced at 750 °C 1h. The long-term stability test was finally carried out at 700 °C for 24 h (Figure 6b). Both reactants, CH_4 and CO_2, exhibit relatively high initial conversions, followed by a rapid decline during the first few hours on stream. CO_2 conversion decreases sharply from its initial value to approximately 40-45% within the first 2-3 h, whereas CH_4 conversion shows an even more pronounced early drop, falling from about 55-60% to below 30% over the same period.

 doi:10.20944/preprints202601.0953.v1

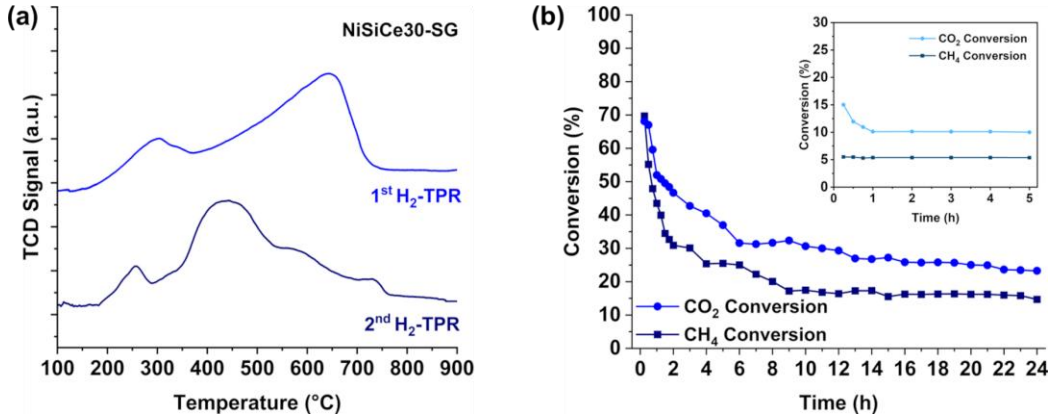

Figure 6. (a) First and second H_2-TPR profiles of NiSiCe30-SG recorded in consecutive TPR/TPO/TPR experiments; (b) DRM long run tests at 700 °C of NiSiCe30-SG after a complete redox cycle (reduction at 750 °C, reoxidation at 600 °C, second reduction at 750 °C). Inset: DRM test at 700 °C of the NiSiCe30-SG after only one reduction at 750 °C.

The initially high activity indicates that the second reduction treatment is beneficial for the reorganization of the Ni active sites, which are likely more dispersed and more accessible on the catalyst surface. However, the catalyst undergoes rapid deactivation within the first 1-2 h, probably due to modifications of the active sites, such as metal sintering, which affect CH_4 activation more severely than CO_2 activation. After this transient period, both conversion curves gradually approach a quasi-steady state. Between approximately 6 and 24 h on stream, CO_2 conversion stabilizes at around 23-27%, while CH_4 conversion levels off at lower values, ca. 14-17%. Throughout the entire test, CO_2 conversion remains consistently higher than that of CH_4, in agreement with previous observations (see Figures 3 and 5). In the Figure 6b (inset), the CH_4 and CO_2 conversion profiles recorded at 700 °C over the same NiSiCe30-SG catalyst after a single reduction treatment at 750 °C, are displayed during the first 5 h of reaction. This behavior confirms the poor catalytic activity previously observed under temperature-programmed conditions. In this case, CO_2 conversion decreases modestly from ~15% to ~10% within the first hour and then remains nearly constant, whereas CH_4 conversion stays close to ~5% over the entire 5 h interval.

The influence of the support synthesis method on the catalytic performance was evaluated for NiSiCe5-WI and NiSiCe30-WI catalysts by performing gradient temperature tests between 450 °C and 750 °C. For reference, the catalytic results of the corresponding sol-gel (SG) samples (Figure 3) are included in Figure 7a, providing a comprehensive comparison of all catalysts prepared from SiCe supports with 5 wt% and 30 wt% ceria. Both NiSiCe5-WI and NiSiCe30-WI exhibit higher CH_4 conversions than NiSi and the NiSiCe(5-30)-SG samples, with NiSiCe5-WI achieving the highest conversion. The H_2/CO values for both the NiSiCe-WI catalysts lie between 0.7 and 0.8 in the 500–700 °C range, remaining lower than those of the SG series samples. At 750 °C, the curves intersect those of NiSi and the NiSiCe-SG at the same value of 1 (see inset, Figure 7a).

 doi:10.20944/preprints202601.0953.v1

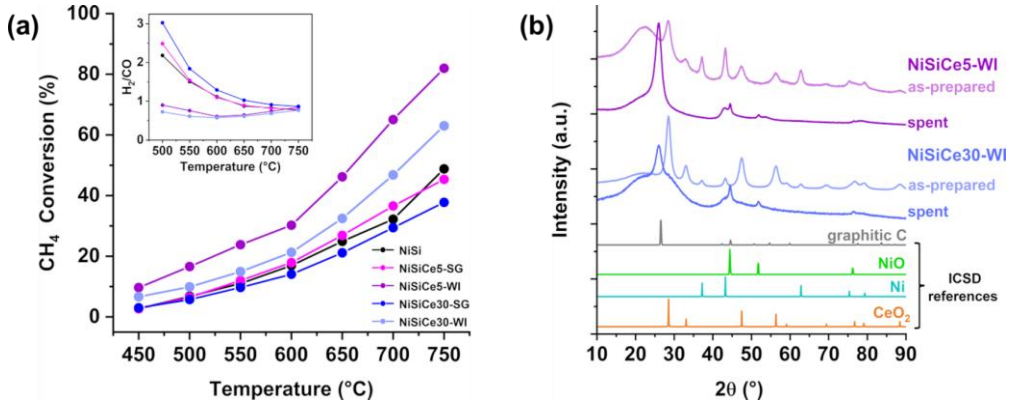

Figure 7. (a) DRM results (CH_4 conversion and H_2/CO ratio) as a function of temperature between 450-750 °C for NiSiCe5,30WI and NiSiCe5,30SG; (b) XRD patterns of the as-prepared and spent NiSiCe5-WI and NiSiCe30-WI, ICSD references (metallic Ni No. 125689, CeO_2 No. 28753, graphitic C No. 53781).

The spent NiSiCe5,30-WI catalysts were subsequently characterized by XRD and TG analyses, which revealed the presence of carbon deposits (Figures 7b, 8b). The XRD patterns again displayed the main diffraction peak of graphitic carbon, while CeO_2 diffraction peaks were not detected, according with previous findings.

Based on these findings, the catalytic stability of NiSiCe5-WI and NiSiCe30-WI was further assessed in a 24 h DRM test at 700 °C (Figure 8a). NiSiCe5-WI exhibited the highest activity, achieving initial CH_4 and CO_2 conversions of 85% and 79%, respectively. These values exceed those obtained under gradient temperature conditions by 39% and 14%, respectively (Figure 7a), indicating that NiSiCe5-WI performs efficiently at 700 °C during long-term conditions.

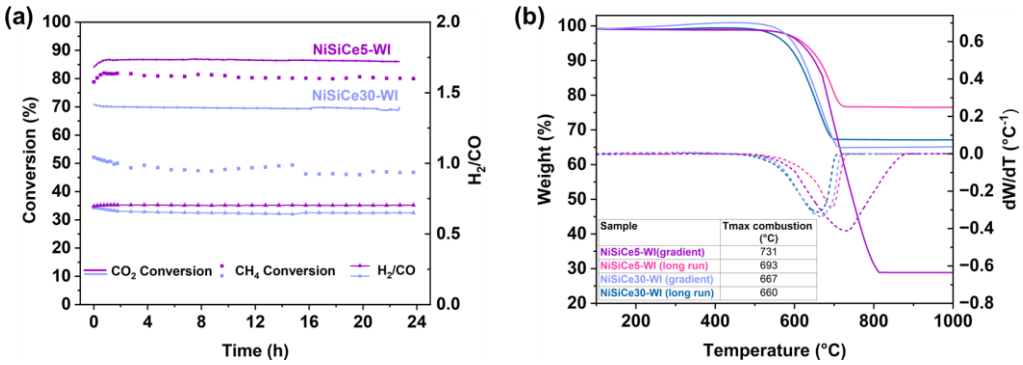

Figure 8. (a) DRM long run tests at 700 °C for Ni-SiCe5-WI and NiSiCe30-WI; (b) TGA profiles of the spent Ni-SiCe5-WI and NiSiCe30-WI after gradient and long run tests.

Raman spectra of the as-prepared and spent NiSiCe5,30-SG and NiSiCe5,30-WI catalysts were recorded to investigate additional structural features (Figure 9), complementing the XRD findings. For all samples, the resulting spectra exhibit a peak centered at 483 cm^{-1}, which is ascribed to the stretching vibration of Si-O-Si bonds[29].

For the spent catalysts, the intensity of this peak is markedly reduced, suggesting partial coverage or blockage of the silica framework. This effect could be likely caused by carbon deposition formed during the DRM reactions, which can hinder the detection of Si–O–Si vibrations and may also affect the structural integrity and accessibility of the active sites. The F_{2g} vibration mode of the CeO_2 fluorite structure was clearly detected at ~462 cm^{-1} for the as-prepared NiSiCe5-WI and NiSiCe30-SG. The sharper peak observed for the as-prepared NiSiCe5-WI is consistent with its higher crystallinity[30], which can be attributed to the synthesis method. In contrast, the F_{2g} peak was not

 doi:10.20944/preprints202601.0953.v1

detected in the NiSiCe5-SG analogue, reflecting the highly dispersed and poorly crystalline nature of CeO_2 resulting from the sol-gel synthesis of the bare SiCe5-SG support.

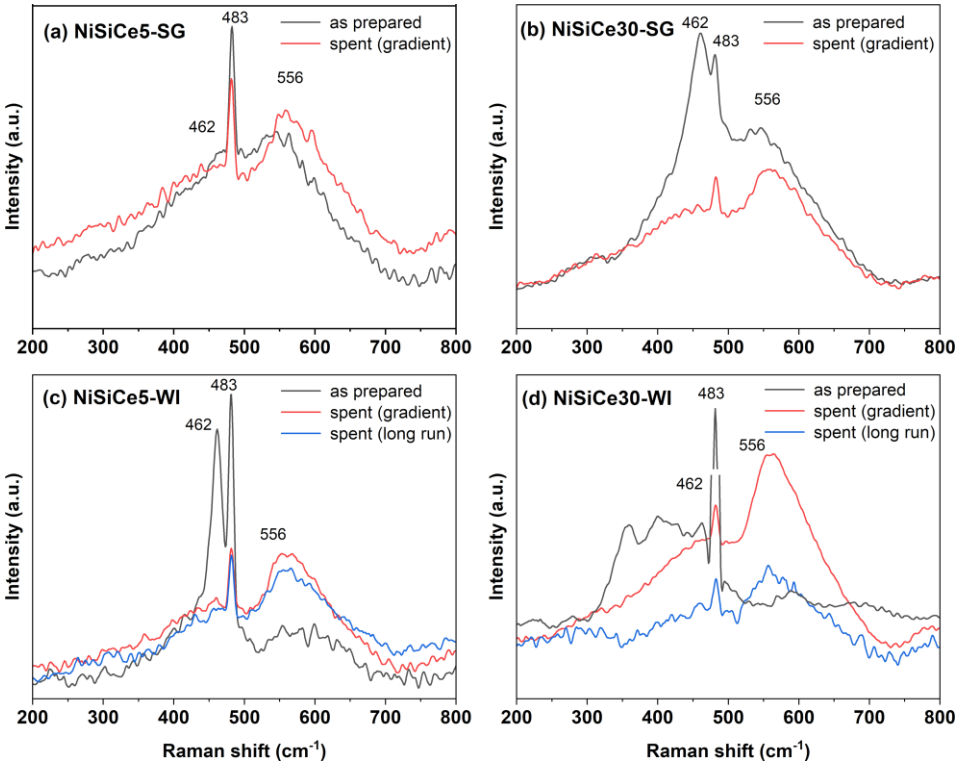

Figure 9. (a) Raman spectra of the as-prepared and spent catalysts: (a) NiSiCe5-SG, (b) NiSiCe30-SG, (c) NiSiCe5-WI, (d) NiSiCe30-WI.

Consistently with the XRD analysis, the characteristic F_2g Raman mode of CeO_2 is not clearly detected in the spent catalysts after DRM, which may be attributed to the combined effects of carbon deposition and a reduction in the long-range order of ceria domains during reaction. The D_1 bands observed in the 500-600 cm^{-1} range are ascribed bulk oxygen vacancies (O_{v-b}) in the ceria fluorite structure[31]. These bands reflect the presence of local structural defects in CeO_2, which are likely related to the presence of Ce^{3+} species. Moreover, the D_1 band of the spent catalysts appears more pronounced than in the corresponding as-prepared samples, indicating that DRM conditions induce additional oxygen vacancies and structural disorder. Qualitatively, while the F_{2g} band of CeO_2 reflects the long-range fluorite order, the relative prominence of the D_1 band in the spent samples suggests an increase in defect density. Among the catalysts studied, NiSiCe5 WI exhibits the strongest D_1 signal, consistent with a higher concentration of bulk oxygen vacancies, which may contribute to its superior catalytic performance[32].

Raman spectroscopy was also employed to elucidate the nature and structural order of the carbon deposits on the spent catalysts after DRM focusing on the 1260-1680 cm^{-1} Raman shift range (Figure 10). The spectra of the spent catalysts exhibit the characteristic G band at ~1588 cm^{-1}, associated with the E_{2g} vibration of sp^2 carbon, and the D band at ~1309-1352 cm^{-1}, which becomes active in the presence of defects or structural disorder. The I_D/I_G ratio was calculated to assess the degree of disorder versus graphitization in the deposited carbon, as it is widely used to quantify the structural quality of sp^2 carbon materials[33,34].

Higher values denote a more defective carbon network, whereas lower ratios indicate increased ordering. The catalysts recovered after the temperature-gradient test exhibit I_D/I_G values of NiSiCe5-WI (1.21) > NiSiCe30-SG (1.17) > NiSiCe5-SG (1.14) > NiSiCe30-WI (1.10), indicating that NiSiCe30-WI accumulates the most graphitized carbon. After the long-term stability test, the I_D/I_G values

 doi:10.20944/preprints202601.0953.v1

converge (1.06 for NiSiCe5-WI and 1.05 for NiSiCe30-WI), suggesting that extended operation promotes the formation of similarly ordered carbon species.

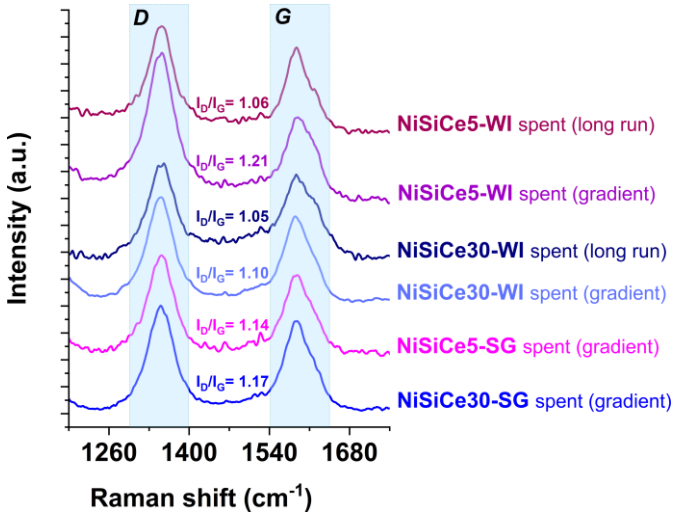

Figure 10. Raman spectra of the spent catalysts after DRM tests.

3. Materials and Methods

3.1. Synthesis Procedures of Si-SG, SiCe(5-30)-SG, SiCe(5-30)-WI and the Corresponding Ni-Based Powders

Bare SiO_2 (Si-SG) and SiO_2-CeO_2 mixed oxides (SiCe(5-30)-SG) were prepared via a sol-gel method. For the synthesis of pure SiO_2, TEOS (11 mL) was first dissolved in 8.5 mL of ethanol under magnetic stirring at room temperature. To this solution, 8 mL of an acetic acid solution (pH = 6) were added dropwise under continuous stirring. The resulting mixture was then heated to 45 °C for 1 h and subsequently to 80 °C for an additional hour. After heating, the sol was cooled to room temperature and kept overnight to promote gelation. The resulting gel was manually crushed at 80 °C and dried at 100 °C overnight. The dried material was then ground and calcined at 450 °C for 4 h (2 °C min^{-1}).

The SiCe(5-30)-SG materials were prepared following the same procedure, adding the appropriate amounts of cerium (III) nitrate ($Ce(NO_3)_3{\cdot}6H_2O$) as the cerium oxide precursor to the silica sol solution to obtain final ceria loadings of 5%, 10%, 20%, and 30% (w/w).

SiCe5-WI and SiCe30-WI were prepared by sequential wetness impregnation of the bare Si-SG with an aqueous solution of cerium nitrate. The resulting materials were dried at 100 °C and calcined at 450 °C with a heating rate of 2 °C min^{-1} for 4 h.

All Ni-containing catalysts, based on both the unmodified and Ce-modified supports, were synthesized by sequential wetness impregnation using an aqueous solution of $Ni(NO_3)_2{\cdot}6H_2O$. The nominal nickel loading was 5 wt%. The catalyst samples were dried at 100 °C and calcined under static conditions at 600 °C with a heating rate of 2 °C min^{-1} for 4 h (as-prepared samples).

3.2. Characterization of the Materials

Specific surface areas and pore volumes were determined from N_2 adsorption-desorption isotherms measured at -196 °C using an ASAP 2020 instrument (Micromeritics, Norcross, GA, USA). Prior to analysis, the samples were degassed at 250 °C for 2 h. Surface areas were calculated using the Brunauer-Emmett-Teller (BET) method over the relative pressure range 0.05-0.30 (P/P_0). Pore volumes and pore size distributions were obtained from the desorption branch using the Barrett-Joyner-Halenda (BJH) method.

Powder X-ray diffraction (XRD) patterns were collected on a D5000 diffractometer (Bruker AXS, Karlsruhe, Germany) using Ni-filtered Cu Kα radiation. Data were recorded over the 2θ range 10-

 doi:10.20944/preprints202601.0953.v1

90° with a step size of 0.05°. Phase identification was performed using the ICSD database (Inorganic Crystal Structure Database, version 5.5.0), and crystallite sizes were calculated using the Scherrer equation applied to the main reflections[35].

Hydrogen temperature-programmed reduction (H_2-TPR) was conducted using an Autochem 2910 system (Micromeritics, Norcross, GA, USA) equipped with a TCD detector. Samples (0.10 g) were pretreated in 5% O_2/He (30 mL min^{-1}) by heating to 400 °C at 10 °C min^{-1} and holding for 30 min. After cooling to room temperature under He flow (30 mL min^{-1}), reduction was carried out in 5% H_2/Ar (30 mL min^{-1}) up to 900 °C at 10 °C min^{-1}. H_2 consumption was quantified by integration of the TPR peaks using a calibration curve obtained from different H_2/Ar gas mixtures. The uncertainty in hydrogen consumption measurements was ±2%. Consecutive temperature-programmed reduction/temperature-programmed oxidation (TPR/TPO) and subsequent TPR experiments were conducted by oxidizing at 600 °C 1h with 5% O_2/He (30 mL min^{-1}) the previously reduced sample followed by cooling to room temperature under He flow. A subsequent TPR run was then performed under identical conditions, as above described.

Raman spectra of the powders were recorded using a Thermo Fisher Scientific DXR3 Raman spectrometer with a 532 nm excitation laser and a laser power of 0.2 mW.

3.3. DRM Catalytic Tests

The dry reforming of methane (DRM) reaction was performed in a fixed-bed quartz reactor (inner diameter: 12 mm) operating at atmospheric pressure. Catalytic tests were conducted as a function of the temperature, in the temperature range 450–750 °C, using 50 °C increments. Tests were also carried out at 700 °C for 24 h of time on the stream (TOS) to evaluate the stability in catalytic conversion.

Typically, for each catalytic, test 100 mg of catalyst (sieved to 180-250 μm) were diluted 1:2 with inert SiC and loaded into the reactor. Prior to reaction, each catalyst was treated in 5% O_2/He (v/v, 50 mL min^{-1}) at 350 °C for 30 min to clean the surface and ensure reproducible starting conditions. After cooling to room temperature, the sample was reduced at 750 °C (heating rate of 10 °C min^{-1}) under 5% H_2/He (v/v, 30 mL min^{-1}) and held at this temperature for 1 h. The feed mixture consisted of 10% CH_4, 10% CO_2, and He as balance, introduced at a total flow rate of 100 mL min^{-1} (STP), corresponding to a gas hourly space velocity (GHSV) of 60,000 mL g^{-1} h^{-1}. The inlet and outlet streams were analysed online by an Agilent 7890B gas chromatograph (Agilent Technologies, Santa Clara, CA, USA) equipped with a DB-1 capillary column and a molecular sieve column, using flame ionization (FID) and thermal conductivity (TCD) detectors to monitor CH_4, CO_2, CO, and H_2. Water formed during reaction was condensed at the reactor outlet.

Methane and carbon dioxide conversions (XCH_4 and XCO_2) were calculated using the following equations, where CH_4^{in}, CO_2^{in} and CH_4^{out}, CO_2^{out}, H_2^{out} and CO^{out} denote inlet and outlet concentrations (ppm), respectively:

$$XCH_4 = 100 \times (CH_4^{in} - CH_4^{out})/CH_4^{in}$$

$$XCO_2 = 100 \times (CO_2^{in} - CO_2^{out})/CO_2^{in}$$

4. Conclusions

Nickel catalysts supported on SiO_2-CeO_2 mixed oxides were investigated for methane dry reforming (DRM), focusing on the effects of ceria loading and support synthesis on Ni dispersion, reducibility, catalytic activity, and carbon resistance. The results show that both support composition and preparation method strongly influence the structure-performance relationships of Ni-based catalysts. For sol-gel-derived supports, increasing CeO_2 content (5-30 wt%) enhanced NiO dispersion and reduced crystallite size, indicating stronger metal-support interactions. At low ceria loadings (5-10 wt%), an optimal balance between dispersion and reducibility was achieved, resulting in DRM activity and improved carbon removal due to ceria's redox properties. In contrast, higher CeO_2

 doi:10.20944/preprints202601.0953.v1

contents led to overly strong Ni-CeO_2 interactions, limiting Ni reducibility and accessibility and thus decreasing methane conversion, despite enhanced CO_2 activation.

The sol-gel-derived Ni/SiO_2 catalyst showed the highest activity and good stability at 700 °C, maintaining constant CH_4 and CO_2 conversions over 24 h with minimal carbon deposition, highlighting the benefit of weak-to-moderate metal-support interactions for stabilizing active Ni^0 sites. Redox cycling of the high-ceria NiSiCe30-SG catalyst temporarily improved reducibility and initial activity but resulted in rapid deactivation, likely due to Ni sintering or structural changes. Comparison with wetness-impregnated catalysts revealed a strong preparation effect: although these catalysts preserved silica texture and exhibited higher activity and very high initial conversions, they suffered from increased carbon deposition, particularly ordered graphitic carbon.

Overall, optimal Ni/SiO_2-CeO_2 catalysts for DRM require careful tuning of ceria content and synthesis method. Low ceria loadings introduced via sol-gel synthesis offer the best balance between activity, stability, and coke resistance, providing guidance for the rational design of durable Ni-based DRM catalysts.

Author Contributions: Conceptualization, C.C, V.L.P., G.P. and L.F.L.; methodology, C.C, V.L.P., G.P. and L.F.L.; software, C.C, V.L.P.; validation, C.C, V.L.P., G.P. and L.F.L.; formal analysis, C.C, V.L.P., G.P. and L.F.L.; investigation C.C, V.L.P., G.P. and L.F.L.; data curation, C.C, V.L.P., G.P. and L.F.L; writing—original draft preparation, C.C, and L.F.L writing—review and editing, C.C, V.L.P., G.P. and L.F.L.; visualization, C.C, V.L.P., G.P. and L.F.L. funding acquisition, L.F.L. All authors have read and agreed to the published version of the manuscript.

Funding: The Projects "Accordo di programma per la regolamentazione dei rapporti in relazione allo svolgimento di attività di ricerca nell'ambito del piano nazionale di ripresa e resilienza (PNRR) - missione 2 "rivoluzione verde e transizione ecologica" – componente 2 "energia rinnovabile, idrogeno, rete e mobilità sostenibile" – investimento 3.5 "ricerca e sviluppo sull'idrogeno" - AdP ENEA CNR (CUP B93C22000630006) and Programma di Ricerca e Innovazione dal titolo "NEST - Network 4 Energy Sustainable Transition", (Partenariato Esteso – PE0000021, CUP B53C22004060006) are acknowledged for financial support.

Data Availability Statement: The original contributions presented in this study are included in the article. Further inquiries can be directed to the corresponding author(s).

Acknowledgments: The authors are thankful to Francesco Giordano (CNR-ISMN) for performing XRD analyses and to Nunzio Galli (CNR-ISMN) for performing N_2 physisorption measurements.

Conflicts of Interest: The authors declare no conflicts of interest.

References

1. Gholami, Z.; Gholami, F.; Šimek, J.; Svobodová, K.; Vakili, M. Hydrogen production for a decarbonized future: a review of production technologies. *Journal of Industrial and Engineering Chemistry* **2026**, *153*, 240-278, https://doi.org/10.1016/j.jiec.2025.07.047.
2. Wittich, K.; Krämer, M.; Bottke, N.; Schunk, S.A. Catalytic Dry Reforming of Methane: Insights from Model Systems. *ChemCatChem* **2020**, *12*, 2130-2147, https://doi.org/10.1002/cctc.201902142.
3. Agún, B.; Abánades, A. Comprehensive review on dry reforming of methane: Challenges and potential for greenhouse gas mitigation. *International Journal of Hydrogen Energy* **2025**, *103*, 395-414, https://doi.org/10.1016/j.ijhydene.2025.01.160.
4. Nguyen, D.L.T.; Vy Tran, A.; Vo, D.-V.N.; Tran Nguyen, H.; Rajamohan, N.; Trinh, T.H.; Nguyen, T.L.; Le, Q.V.; Nguyen, T.M. Methane dry reforming: A catalyst challenge awaits. *Journal of Industrial and Engineering Chemistry* **2024**, *140*, 169-189, https://doi.org/10.1016/j.jiec.2024.06.017.
5. Osazuwa, O.U.; Ng, K.H. An overview on the carbon deposited during dry reforming of methane (DRM): Its formation, deposition, identification, and quantification. *Results in Engineering* **2025**, *25*, 104328, https://doi.org/10.1016/j.rineng.2025.104328.

 doi:10.20944/preprints202601.0953.v1

6. Wang, Z.; Mei, Z.; Wang, L.; Wu, Q.; Xia, C.; Li, S.; Wang, T.; Liu, C. Insight into the activity of Ni-based thermal catalysts for dry reforming of methane. *Journal of Materials Chemistry A* **2024**, *12*, 24802-24838, doi:10.1039/D4TA04069D.
7. Xu, Z.; Park, E.D. Recent Advances in Coke Management for Dry Reforming of Methane over Ni-Based Catalysts. *Catalysts* **2024**, *14*, 176, doi:10.3390/catal14030176.
8. Zhu, H.; Chen, H.; Zhang, M.; Liang, C.; Duan, L. Recent advances in promoting dry reforming of methane using nickel-based catalysts. *Catalysis Science & Technology* **2024**, *14*, 1712-1729, doi:10.1039/D3CY01612A.
9. Shi, Y.; Tian, X.; Deng, Z.; Shi, W.; Fan, W.; Wang, F. Review and Outlook of Confined Ni Catalysts for the Dry Reforming of Methane Reaction. *Energy & Fuels* **2024**, *38*, 1633-1656, doi:10.1021/acs.energyfuels.3c03923.
10. Chen, C.; Wei, J.; Lu, Y.; Duyar, M.S.; Huang, Y.; Lin, L.; Ye, R. Confinement effects over Ni-based catalysts for methane dry reforming. *Catalysis Science & Technology* **2023**, *13*, 6089-6101, doi:10.1039/D3CY00845B.
11. Montini, T.; Melchionna, M.; Monai, M.; Fornasiero, P. Fundamentals and Catalytic Applications of CeO2-Based Materials. *Chemical Reviews* **2016**, *116*, 5987-6041, doi:10.1021/acs.chemrev.5b00603.
12. Teh, L.P.; Setiabudi, H.D.; Timmiati, S.N.; Aziz, M.A.A.; Annuar, N.H.R.; Ruslan, N.N. Recent progress in ceria-based catalysts for the dry reforming of methane: A review. *Chemical Engineering Science* **2021**, *242*, 116606, https://doi.org/10.1016/j.ces.2021.116606.
13. Niu, Y.; Zheng, X.; Guo, B.; Liu, H.; Jin, Y.; Niu, J. Particle size tuning of Ni/CeO2 catalysts and their performance in methane dry reforming reaction. *Gas Science and Engineering* **2026**, *145*, 205790, https://doi.org/10.1016/j.jgsce.2025.205790.
14. Janlon, J.; Chatsuwan, N.; Kongparakul, S.; Ratthiwal, J.; Fong, Y.Y.; Reubroycharoen, P.; Chanlek, N.; Tran, T.T.V.; Samart, C. Highly stable Ni-based catalysts supported on silica nanofibers for the dry reforming of methane with CO2-rich feedstock. *Journal of the Energy Institute* **2025**, *123*, 102313, https://doi.org/10.1016/j.joei.2025.102313.
15. Zhang, Y.; Liu, J.; Zhang, G.; Zhang, X.; Wang, Y.; Zhao, Y.; Li, G. Ni/MSS@CeO2 sandwich catalysts for methane dry reforming: the role of reduction on oxygen vacancies. *Journal of Colloid and Interface Science* **2025**, *694*, 137712, https://doi.org/10.1016/j.jcis.2025.137712.
16. Li, Y.; Li, Z.; Wang, N.; Zha, Y.; Zheng, K.; Xu, Y.; Liu, B.; Liu, X. Strong activity-based volcano-type relationship for dry reforming of methane through modulating Ni-CeO2 interaction over Ni/CeO2-SiO2 catalysts. *Chem Catalysis* **2025**, *5*, 101189, https://doi.org/10.1016/j.checat.2024.101189.
17. Cherevotan, A.; Ray, B.; Churipard, S.R.; Kaur, K.; Gautam, U.K.; Vinod, C.P.; Peter, S.C. Influence of support textural property on CO2 to methane activity of Ni/SiO2 catalysts. *Applied Catalysis B: Environmental* **2022**, *317*, 121692, https://doi.org/10.1016/j.apcatb.2022.121692.
18. Zhang, Y.; Zhang, G.; Liu, J.; Li, T.; Wang, Y.; Zhao, Y.; Li, G.; Zhang, Y. Dry reforming of methane over Ni/SiO2 catalysts: Role of support structure properties. *Fuel* **2023**, *340*, 127490, https://doi.org/10.1016/j.fuel.2023.127490.
19. Gao, S.; Li, Y.; Guo, W.; Ding, X.; Zheng, L.; Wu, L.; Yan, H.; Wang, Y. Morphology effect of ceria support with hierarchical structure on the catalytic performance for nickel-based catalysts in dry reforming of methane. *Molecular Catalysis* **2022**, *533*, 112766, https://doi.org/10.1016/j.mcat.2022.112766.
20. Han, K.; Xu, S.; Wang, Y.; Wang, S.; Zhao, L.; Kambonde, J.; Yu, H.; Shi, W.; Wang, F. Confining Ni and ceria in silica shell as synergistic multifunctional catalyst for methane dry reforming reaction. *Journal of Power Sources* **2021**, *506*, 230232, https://doi.org/10.1016/j.jpowsour.2021.230232.
21. Liu, Z.; Grinter, D.C.; Lustemberg, P.G.; Nguyen-Phan, T.-D.; Zhou, Y.; Luo, S.; Waluyo, I.; Crumlin, E.J.; Stacchiola, D.J.; Zhou, J.; et al. Dry Reforming of Methane on a Highly-Active Ni-CeO2 Catalyst: Effects of Metal-Support Interactions on C−H Bond Breaking. *Angewandte Chemie International Edition* **2016**, *55*, 7455-7459, https://doi.org/10.1002/anie.201602489.
22. Li, B.; Yuan, X.; Li, B.; Wang, X. Ceria-modified nickel supported on porous silica as highly active and stable catalyst for dry reforming of methane. *Fuel* **2021**, *301*, 121027, https://doi.org/10.1016/j.fuel.2021.121027.
23. Zhou, Q.; Fu, X.; Hui Lim, K.; Li, Z.; Liao, M.; Lu, J.; Liu, F.; Kawi, S. Complete confinement of Ce/Ni within SiO2 nanotube with high oxygen vacancy concentration for CO2 methane reforming. *Fuel* **2022**, *325*, 124819, https://doi.org/10.1016/j.fuel.2022.124819.

 doi:10.20944/preprints202601.0953.v1

24. Grabchenko, M.V.; Dorofeeva, N.V.; Svetlichnyi, V.A.; Larichev, Y.V.; La Parola, V.; Liotta, L.F.; Kulinich, S.A.; Vodyankina, O.V. Ni-Based SBA-15 Catalysts Modified with CeMnOx for CO2 Valorization via Dry Reforming of Methane: Effect of Composition on Modulating Activity and H2/CO Ratio. *Nanomaterials* **2023**, *13*, 2641, doi:10.3390/nano13192641.
25. La Parola, V.; Liotta, L.F.; Pantaleo, G.; Testa, M.L.; Venezia, A.M. CO2 reforming of CH4 over Ni supported on SiO2 modified by TiO2 and ZrO2: Effect of the support synthesis procedure. *Applied Catalysis A: General* **2022**, *642*, 118704, https://doi.org/10.1016/j.apcata.2022.118704.
26. Ali, S.; Khader, M.M.; Almarri, M.J.; Abdelmoneim, A.G. Ni-based nano-catalysts for the dry reforming of methane. *Catalysis Today* **2020**, *343*, 26-37, https://doi.org/10.1016/j.cattod.2019.04.066.
27. Taufiq-Yap, Y.H.; Sudarno; Rashid, U.; Zainal, Z. CeO2–SiO2 supported nickel catalysts for dry reforming of methane toward syngas production. *Applied Catalysis A: General* **2013**, *468*, 359-369, https://doi.org/10.1016/j.apcata.2013.09.020.
28. Sudarno; Razali, S.M.; Asikin-Mijan, N.; Sivasangar, S.; Taufiq-Yap, Y.H. Enhanced dry reforming toward hydrogen production over Ni/CeO2SiO2 via different catalyst synthesis routes. *International Journal of Hydrogen Energy* **2019**, *44*, 20738-20750, https://doi.org/10.1016/j.ijhydene.2018.12.018.
29. Peszke, J.; Dulski, M.; Nowak, A.; Balin, K.; Zubko, M.; Sułowicz, S.; Nowak, B.; Piotrowska-Seget, Z.; Talik, E.; Wojtyniak, M.; et al. Unique properties of silver and copper silica-based nanocomposites as antimicrobial agents. *RSC Advances* **2017**, *7*, 28092-28104, doi:10.1039/C7RA00720E.
30. Kosacki, I.; Suzuki, T.; Anderson, H.U.; Colomban, P. Raman scattering and lattice defects in nanocrystalline CeO2 thin films. *Solid State Ionics* **2002**, *149*, 99-105, https://doi.org/10.1016/S0167-2738(02)00104-2.
31. Grabchenko, M.V.; Mamontov, G.V.; Zaikovskii, V.I.; La Parola, V.; Liotta, L.F.; Vodyankina, O.V. Design of Ag-CeO2/SiO2 catalyst for oxidative dehydrogenation of ethanol: Control of Ag–CeO2 interfacial interaction. *Catalysis Today* **2019**, *333*, 2-9, https://doi.org/10.1016/j.cattod.2018.05.014.
32. Dong, F.; Meng, Y.; Han, W.; Zhao, H.; Tang, Z. Morphology effects on surface chemical properties and lattice defects of Cu/CeO2 catalysts applied for low-temperature CO oxidation. *Scientific Reports* **2019**, *9*, 12056, doi:10.1038/s41598-019-48606-2.
33. Zhang, C.C.; Hartlaub, S.; Petrovic, I.; Yilmaz, B. Raman Spectroscopy Characterization of Amorphous Coke Generated in Industrial Processes. *ACS Omega* **2022**, *7*, 2565-2570, doi:10.1021/acsomega.1c03456.
34. Szybowicz, M.; Nowicka, A.B.; Dychalska, A. Chapter 1 - Characterization of Carbon Nanomaterials by Raman Spectroscopy. In *Characterization of Nanomaterials*, Mohan Bhagyaraj, S., Oluwafemi, O.S., Kalarikkal, N., Thomas, S., Eds.; Woodhead Publishing: 2018; pp. 1-36.
35. Gil, S.; Garcia-Vargas, J.M.; Liotta, L.F.; Pantaleo, G.; Ousmane, M.; Retailleau, L.; Giroir-Fendler, A. Catalytic Oxidation of Propene over Pd Catalysts Supported on CeO2, TiO2, Al2O3 and M/Al2O3 Oxides (M = Ce, Ti, Fe, Mn). *Catalysts* **2015**, *5*, 671-689, doi:10.3390/catal5020671.